GILDAS Imaging Simulations to Investigate the Optimal ACA Observing Time

Shigehisa Takakuwa*, Daisuke Iono, Baltasar Vila-Vilaro, Takahiro Tsutsumi, Koh-Ichiro Morita, & Ryohei Kawabe

ALMA Project Office, National Astronomical Observatory of Japan, Osawa 2-21-1, Mitaka, Tokyo, 181-8588, Japan

(Received ; accepted)

Abstract

We have performed thorough imaging simulations with the GILDAS imaging simulator to search for the optimal ACA observing time required to obtain the maximum fidelity for a given 12-m array observing time. Our simulations adopt two model images ("hco43" and "cluster") at two different declinations of -23° and +20°, and vary the ACA observing time with a fixed 12-m time (Hour Angle = -0.5 – +0.5 hours) and vice versa and then compute imaging fidelities and *uv* fidelities as a function of the ACA and 12-m observing time. In the "high S/N" case ($> 170\ \sigma$ at the 1% level of the peak flux), there is no clear dependence of the fidelity on the ACA observing time with the fixed 12-m observing time, while in the "low S/N" case ($\sim 1.4\ \sigma$) the fidelity increases monotonically as the ACA and/or 12-m array observing time increases. All of these simulations suggest that, although inclusion of the ACA can significantly improve the imaging quality, there is no clear optimal ACA observing time as compared to the 12-m observing time, and that we should seriously consider the mode of the "combined array", which takes cross correlation between the 12-m array and the ACA 7-m array.

Key words: ACA, Imaging Simulations, Combined Array

1. Introduction

The Japanese ALMA group will construct the Atacama Compact Array (ACA), which consists of twelve 7-m antennas as an interferometric array (the ACA 7-m Array) and four 12-m antennas as a total-power array (the ACA TP Array). The ACA can recover missing short-spacing information which the 12-m array cannot sample (< 12 m), significantly enhancing the imaging capability of ALMA. Tsutsumi et al. (2004) have shown that the inclusion of the ACA

* e-mail: s.takakuwa@nao.ac.jp

improves the imaging fidelity to better than 20 for extended sources and specific models. Here, the imaging fidelity ($\equiv F(i,j)$ for each image pixel i,j) is defined as;

$$F(i,j) = \frac{|Model(i,j)|}{max(|Diff(i,j)|, 0.7 \times rms(Diff(i,j)))}, \quad (1)$$

$$Diff(i,j) = Model(i,j) - Simulated(i,j), \quad (2)$$

where $Model(i,j)$ denotes "true" astronomical images as an input to the imaging simulator, $Simulated(i,j)$ "observed" images or output images from the imaging simulator, and $rms(Diff(i,j))$ denotes the rms value of the difference image for the entire image pixel. The fidelity is a quantitative measure of the imaging quality, and higher fidelity values indicate better imaging observations. We can also define the fidelity in the uv-domain, that is, uv fidelity (for detailed discussion on the imaging fidelity and uv fidelity, see Pety et al. 2001c).

However, one important question is how much ACA observing time is required for a given 12-m array observing time, in order to obtain the maximum fidelity and optimum imaging capability. In the imaging simulations by Tsutsumi et al. (2004) the ACA observing time was set to 4 times that of the 12-m array, but they did not investigate whether this value provides the maximum imaging fidelity. Morita & Holdaway (2005) have presented a design concept of the ACA consisting of two configurations; one (Inner Array) is a compact spiral array with small north - south axis ratio ($\times$ 1.1) and the other (NS Array) is a dedicated configuration with large north - south axis ratio ($\sim$ 1.7) (see Figure 1). Their discussion is based on the analyses of the uv-plane sensitivity for mosaicking observations using both the ACA and the 12-m array, and they deduce an optimal ACA observing time of $\sim$ 2.5 – 4 times more than the 12-m observing time. However, the improvements that non-linear algorithms can produce were NOT considered in their calculations. This issue potentially has a significant impact on the ALMA operation. If the required ACA time is similar to that of the 12-m array, we can take cross-correlations between the ACA and 12-m array every time, namely, we can adopt the so-called "combined array" as a routine observing mode. If we need more ACA time than that of the 12-m array for maximum fidelity, we cannot make use of the combined array and we have to make additional ACA observations without the 12-m array. In order to investigate this issue, we have carried out imaging simulations with the GILDAS ALMA imaging simulator developed by Pety and collaborators (Pety et al. 2001a ; Pety et al. 2001b ; Pety et al. 2001c).

2. Simulations

We simulated ALMA imaging with the GILDAS imaging simulator for a range of ACA observing times. We fixed the 12-m observing time to be -0.5 – 0.5 (hour) in Hour Angle, and varied the ACA observing time to be X = 0.5, 1, 1.5 ... 5-times the 12-m observing time. Here, X-times ACA 7-m array observing time denotes that the range of the Hour Angle is -0.5X –

$0.5X$ (hour). The total observing time of the ACA TP array was set to be the same as that of the 7-m array. We also made imaging simulations in the opposite case, that is, we varied the 12-m observing time keeping a fixed ACA observing time. We note that in our simulations the term "observing time" does not represent the simple integration time, but the coverage of hour angles or the *uv* sampling, including the effect of the shadowing. The frequency we adopt is 345 GHz (Band 7). We included thermal noise and random pointing errors of rms $\sim 0.6''$ in all simulations, following the specification of ALMA. Other sources of errors such as instrumental phase noise, atmospheric effect, or any systematic calibration errors are not included in our simulations for simplicity. As model images, we used "hco43" and "cluster" provided by the GILDAS simulator (Pety et al. 2001a ; Pety et al. 2001b ; Pety et al. 2001c). The "hco43" image represents an envelope and disk structure around low-mass protostars (see Figure 4), while the "cluster" image models a star-cluster region (see Figure 5). GILDAS simulations in the literature show that "hco43" and "cluster" represent extreme behavior with respect to the inclusion of the ACA, that is, for the "hco43" image the improvement of the imaging fidelity is the most significant while for the "cluster" image the least significant (Tsutsumi et al. 2004). We adopted the *hybrid* deconvolution algorithm provided by the GILDAS developers, with a maximum clean component of 40000. We did not adopt the full joint deconvolution algorithm to avoid computational overflows. Details of the deconvolution algorithm are described by Pety et al. (2001a, b, c). 7-field mosaicking was performed. In order to obtain statistical significance, we repeated each of the simulations 5 times, and averaged each simulated image and fidelity.

Figure 1 shows the ALMA configuration we adopted for our imaging simulations. The 12-m array is in the most compact configuration, and the center of the ACA antennas is located $\sim$ 150-m north of the 12-m array (Holdaway & Morita 2006). For low elevation sources (-60° $\gtrsim \delta$ or $\delta \gtrsim$ 10°) we adopted the NS-Extended configuration to avoid shadowing. Figure 2 and 3 show the *uv*-coverages and synthesized beams for the configurations shown in Figure 1 at declinations of -23° and +20°, respectively. We adopted Miriad task "*uvgen*" and "*invert*" to calculate these *uv*-coverages and synthesized beams (Sault et al. 1995). Here, the shadowed visibilities with the baseline length shorter than 7-m are flagged by the Miriad task "$uvflag$". In these Figures, the hour angle coverage of both the 12-m array and ACA is from -0.5 to +0.5 (hour). The declination of -23° represents sources which transit at zenith, and the declination of +20° low-elevation sources at the northern hemisphere. The Normal configuration was adopted for the declination of -23°, while the NS-Extended configuration was used for the declination of +20°. The synthesized beam size with natural weighting is $1.21'' \times 1.11''$ (P.A. = -86.5°) and $1.53'' \times 1.21''$ (P.A. = -1.1°) at the declination of -23° and +20°, respectively. Table 1 summarizes the parameters of our simulations.

At $\delta = +20°$, there are shadowed ACA baselines (projected baseline length < 7 m) even with the NS-Extended configuration, and the amount of usable data is not proportional to the hour angle coverage. In Figure 4, we plot the amount of unshadowed ACA data as a function

Table 1. Parameters of the GILDAS Simulations

Parameter	Value
Model Image & Declination	hco43 (δ = -23° and +20°) & cluster (δ = -23°)
Frequency	345 GHz (Band 7)
Number of Mosaics	7 fields
12-m Configuration	Most Compact Configuration
ACA Configuration	Normal (δ = -23°) and NS-Extended (δ = +20°)
12-m Hour Angle	-0.5X – 0.5X (hour), X=0.5,1.0,1.5,...5.0
ACA Hour Angle	-0.5X – 0.5X (hour), X=0.5,1.0,1.5,...5.0
Synthesized Beam (δ = -23°, X = 1.0)	$1.21'' \times 1.11''$ (P.A. = -86.5°)
Synthesized Beam (δ = +20°, X = 1.0)	$1.53'' \times 1.21''$ (P.A. = -1.1°)
Simulation Repetition	5 times
Pointing Error	$0.6''$
Thermal Noise	T_{rec} = 100 K, τ = 0.05, T_{sys}^{tp} = 250 K
Deconvolution	HÖGBOM CLEAN

of the hour angle coverage, as well as the shadowed and unshadowed uv coverages with X = 5. To convert the hour angle coverage into the amount of data, one needs to multiply this percentage by the hour angle coverage. At δ = -23°, there is no shadowing of the ACA and 12-m array within the simulated hour-angle coverage.

3. Simulation Results

3.1. High S/N Case

Figure 5 and 6 show examples of our simulations with the "hco43" and "cluster" model image, respectively. The signal-to-noise ratio (S/N) at the 1 % level of the peak flux reach 680 σ and 170 σ in the case of "hco43" and "cluster", respectively, so the simulations presented below are not susceptible to noise. In these simulations the hour angle coverage of both the 12-m array and ACA is -0.5 – +0.5 (hour), so the ratio of the observing time is unity. The source declination is -23°, and the uv-coverage and the synthesized dirty beam in these simulations are shown in Figure 2. The median imaging fidelities at the 1% cutoff level of the peak intensity with the 12-m array only, the 12-m array and the ACA total power array, the ACA total power array and the ACA 7-m array, and all the array, are listed in Table 2. In the case of "hco43", the extended envelope component is significantly missed by the 12-m array and the median imaging fidelity is below unity. Inclusion of the ACA total power array recovers the extended flux and raises the median imaging fidelity by one order of magnitude. Inclusion of the ACA 7-m array as well as the total power array improves the median fidelity by more than a factor of 6, although Figure 5 does not have enough contrast to see the significant difference between

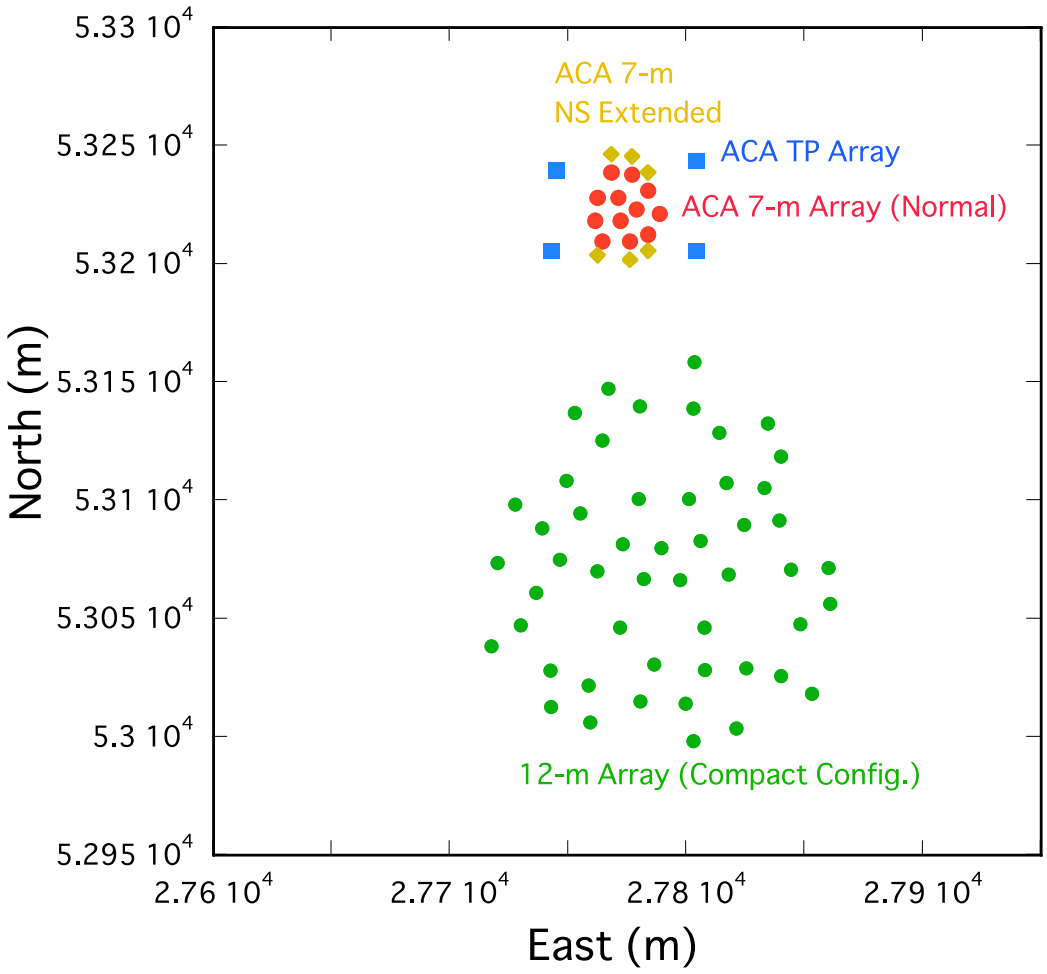

Fig. 1. ALMA antenna locations. Green circles show positions of the 12-m array in the most compact configuration (Conway 2005). Red circles denote positions of the ACA 7-m array in the normal configuration, and orange diamonds in the North-South extended configuration (Morita & Holdaway 2005). Blue squares show positions of the ACA Total Power array.

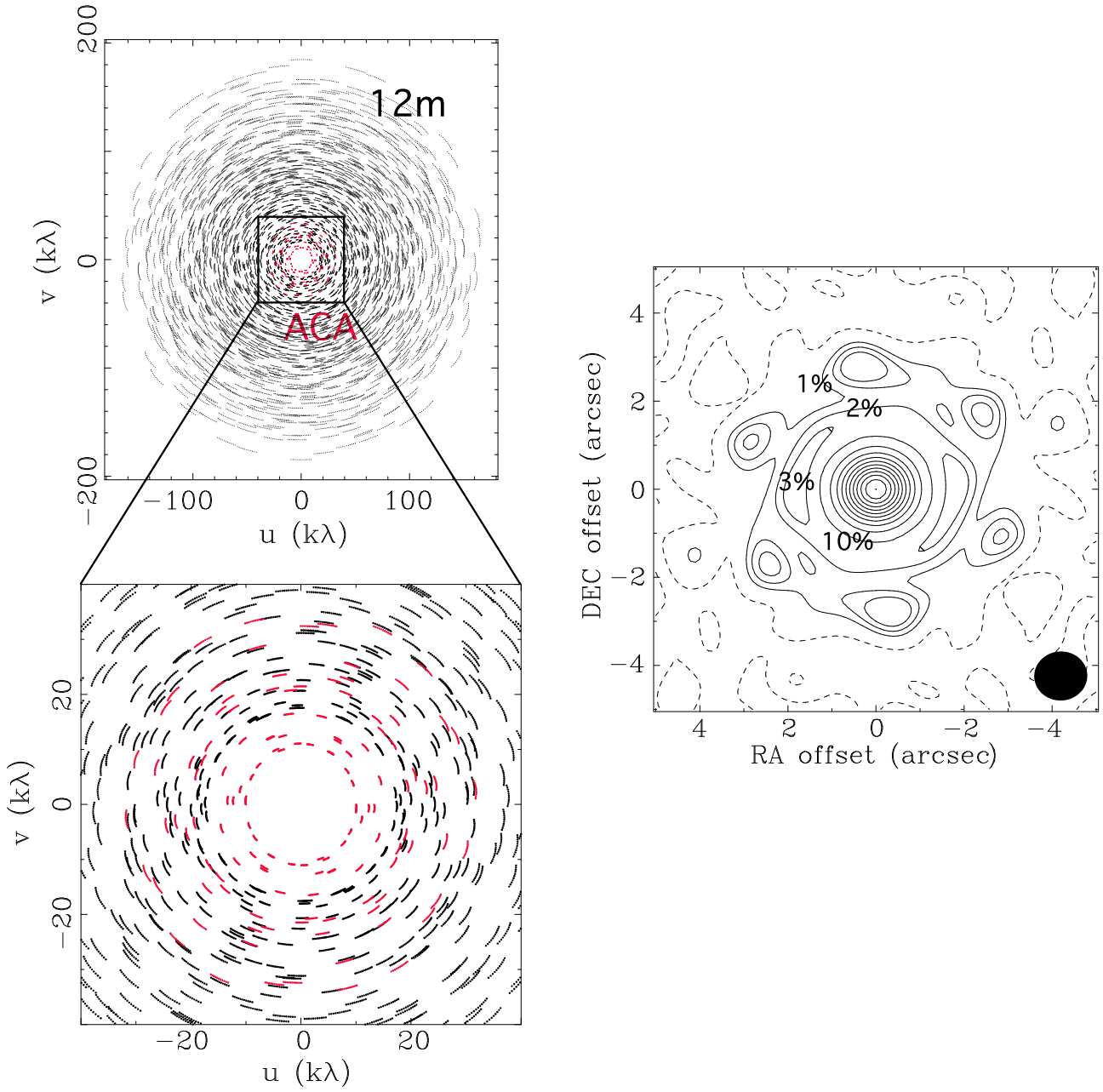

Fig. 2. *uv*-coverage (left panels) and synthesized beam (right) of ALMA for a declination of -23°, that is, the source transits at the zenith. The antenna configuration is shown in Figure 1. The hour angle range is -0.5 – +0.5 (hour) for both the 12-m array and the ACA, and the frequency is 345 GHz. In the left panels, black curves show the *uv*-coverage of the 12-m array and red curves the *uv*-coverage of the ACA 7-m array. In the right panel, the contour levels are 1%, 2%, 3%, 10%, and then every 10% of the peak. Cross correlations between the 12-m and 7-m antennas are not included. The FWHM of the synthesized beam is $1.21'' \times 1.11''$ (P.A. = -86.5°) .

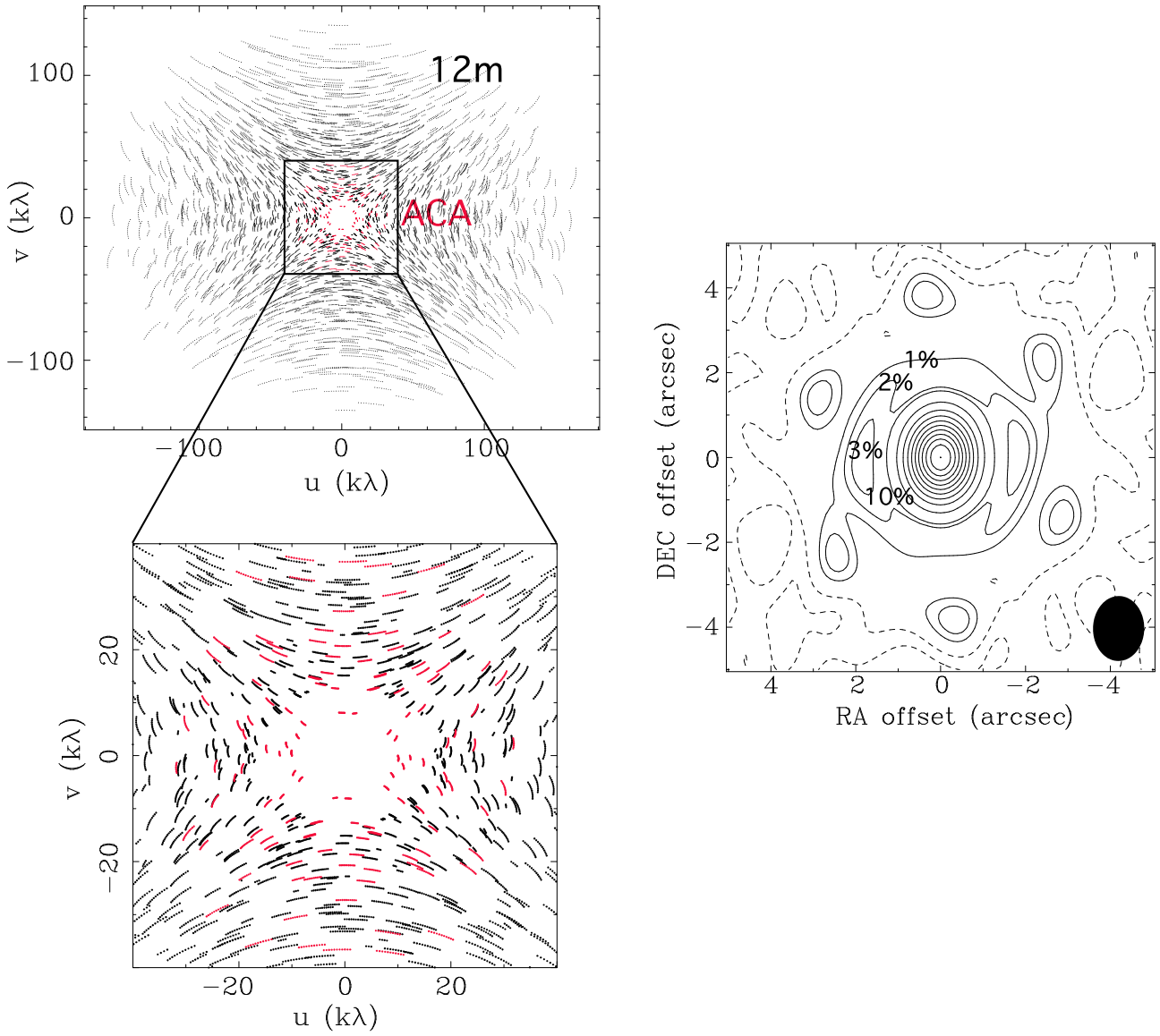

Fig. 3. Same as Figure 2 but for a declination of +20°. The FWHM of the synthesized beam is 1.53″ × 1.21″ (P.A. = -1.1°).

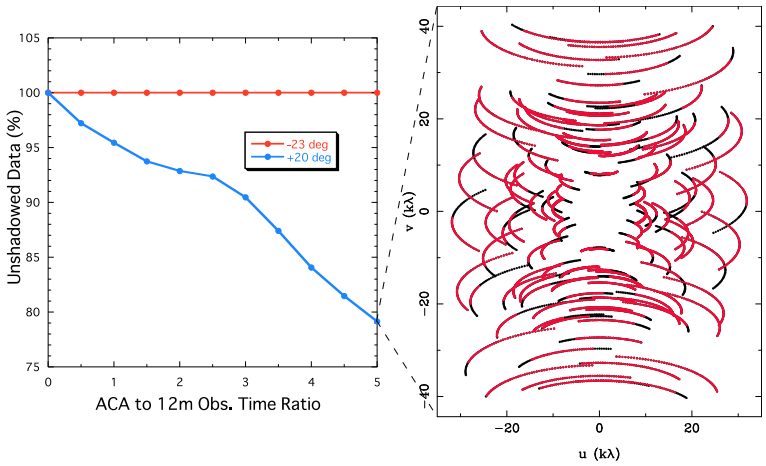

Fig. 4. (left) Amount of unshadowed ACA data as a function of the hour angle coverage at the declination of -23° (red) and +20° (blue). The hour angle coverage is -0.5X – 0.5X (hour), where X is in the abscissa. In our ACA simulations the hour angle coverage of the 12-m array is fixed to -0.5 – 0.5 (hour), so that the abscissa represents the relative observing time between the ACA and the 12-m array. (right) ACA uv coverages of shadowed and unshadowed visibility data. The declination is +20°, and the relative observing time between the ACA and the 12-m array is 5. Red curves show unshadowed uv tracks, while black curves shadowed uv tracks.

the 12-m array + ACA total power array and the 12-m array + all the ACA results. In the case of "cluster", the 12-m array can sample the uv components comprising the detailed source structures, but cannot recover the total flux correctly ($\sim$ 51% flux missed). Inclusion of the ACA total power array can recover both the total flux and the source structures well, and inclusion of the ACA 7-m array provides an additional $\sim$ 20% improvement of the imaging fidelity (Table 2).

Figure 7, 8, 9, 10, and 11 show results of our simulations with varying ACA observing time with respect to the 12-m observing time. Figure 7 and 8 compare images of fidelities at different ACA observing times for the "hco43" and "cluster"image, respectively. The left panels show fidelity images with the same ACA and 12-m array observing time, and the right panels with 4-times more ACA observing time than that of the 12-m array. Comparison between the left and right panels show that there is no noticeable difference of the fidelity images between the different ACA observing times. This trend can be seen more clearly in Figure 9 and 10, which plot median imaging fidelities and uv fidelities as a function of the ratio between the ACA to 12-m observing time in the case of "hco43" and "cluster" models, respectively. In these plots, the zero points in the abscissa represent 12-m array simulations with an hour angle coverage of -0.5 – 0.5 hours. The uv fidelity is defined from the FFT of the model image and the image of the difference between the model image and the simulated image. The dependence of the imaging fidelity and uv fidelity as a function of the time ratio does not show a significant evolution within the rms variations of the simulations. Changing the source declination does

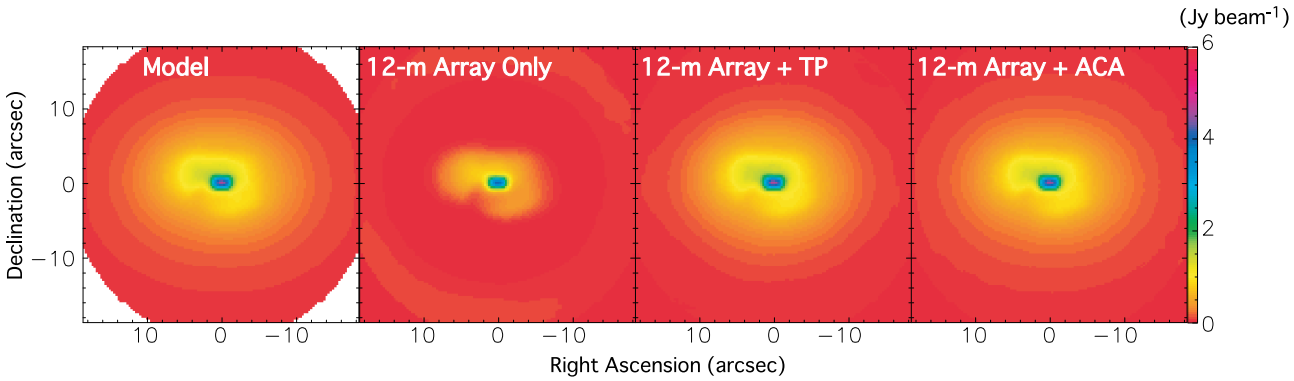

Fig. 5. An example of our imaging simulations with the "hco43" model image. The source declination is -23° and the hour angle coverage is -0.5 – 0.5 (hour) for both the 12-m array and the ACA. The *uv*-coverage and the synthesized dirty beam are shown in Figure 2. The left panel shows the "hco43" model image, the middle-left panel the result of the imaging simulations observed with the 12-m array only, the middle-right panel with the 12-m array plus the Total Power, and the right panel with both the 12-m array and the ACA (the 7-m array and the Total Power). These images are averaged images from 5 repetitions of the simulations.

not alter this trend, as shown in Figure 11. Table 2 summarizes median imaging fidelities of these simulations with a cutoff level of 1 % of the peak. The absolute imaging fidelity in the case of "cluster" is significantly higher than that of "hco43". This is because in the case of "cluster" significant flux is present at longer (> 15 m) spacings than that of "hco43", as seen in the *uv* fidelities in Figure 9 and 10. This means that the 12-m array can make more contribution to improve the imaging quality in the case of "cluster" than "hco43".

These results suggest that, for a "noise-free" case, there is no optimal ACA observing time with a fixed 12-m observing time, and we can just adopt the same observing time for the ACA as that of the 12-m observing time. On the other hand, increasing the 12-m observing time improves the fidelities, as shown in Figure 12. Figure 12 shows that the imaging fidelity and the *uv* fidelity at longer baselines (> 15 m) improves monotonically as the 12-m observing time increases. In Figure 12, the imaging fidelities at the zero point seem to be better than those at the next point with the 12-m array to the ACA observing time ratio of 0.5. However, the spatial resolution between the two points is totally different (at the zero point $\sim 5.3'' \times 4.8''$; at the next point $\sim 1.2'' \times 1.1''$), so the comparison of the imaging fidelities between the two images with and without the 12-m array is misleading, and the comparison of the *uv* fidelities is necessary to properly investigate the effect of the inclusion of the 12-m array.

3.2. Low S/N Case

All the simulations above are high signal-to-noise ratio observations and are independent of noise. In order to investigate the low S/N case, we ran another set of simulations after reducing the flux of "hco43" by a factor of 500 (that is, $\sim 1.4\ \sigma$ at the 1 % level) and "cluster" by a factor of 100 ($\sim 1.7\ \sigma$ at the 1 % level). The results are shown in Figures 13, 14 and

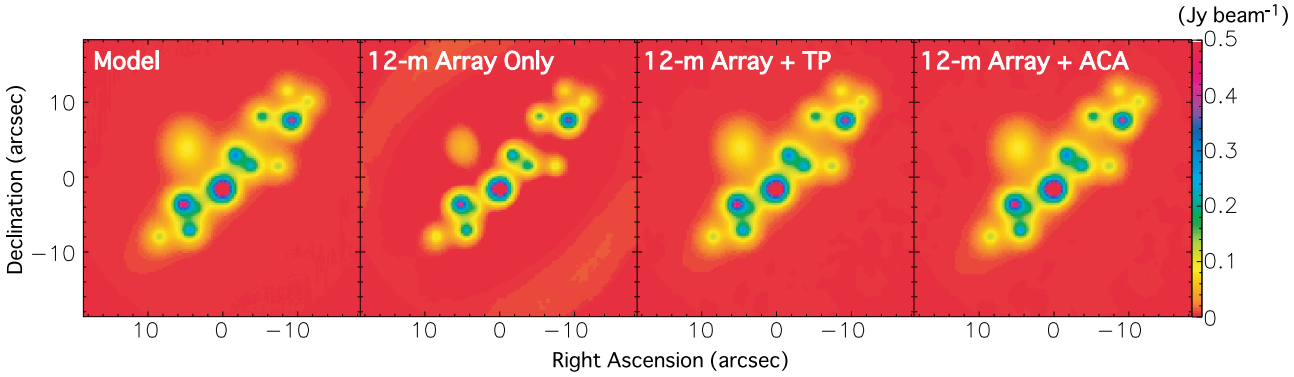

Fig. 6. Same as Figure 5 but for the "cluster" model image.

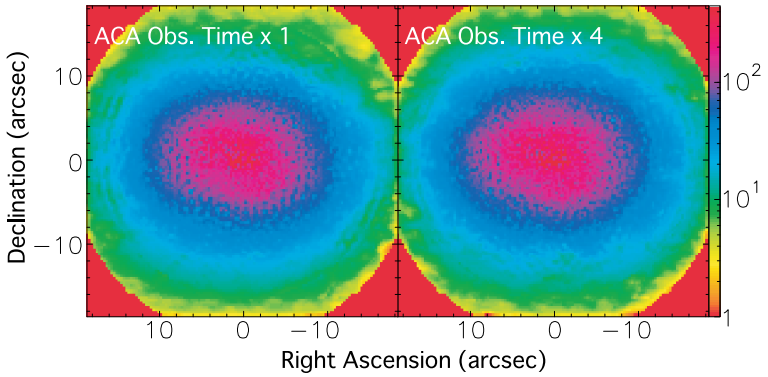

Fig. 7. Averaged fidelity images from 5 imaging simulations of "hco43" with both the 12-m array and the ACA. In the left panel the hour angle coverage of the ACA is -0.5 – 0.5 (hour), while in the right panel -2.0 – 2.0 (hour). The hour angle coverage of the 12-m array is fixed to -0.5 – 0.5 (hour). The source declination is -23°.

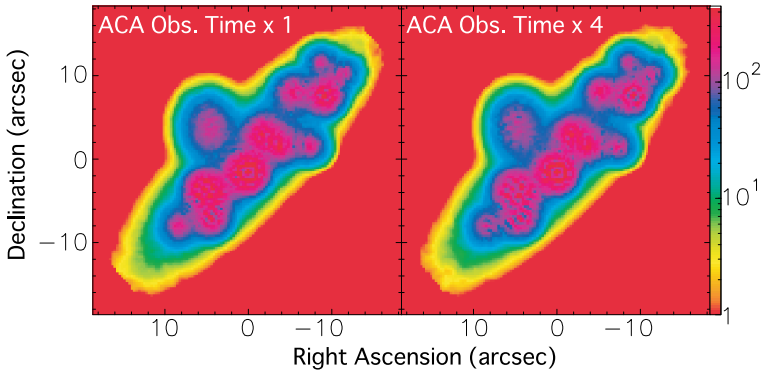

Fig. 8. Same as Figure 7 but for the "cluster" model image.

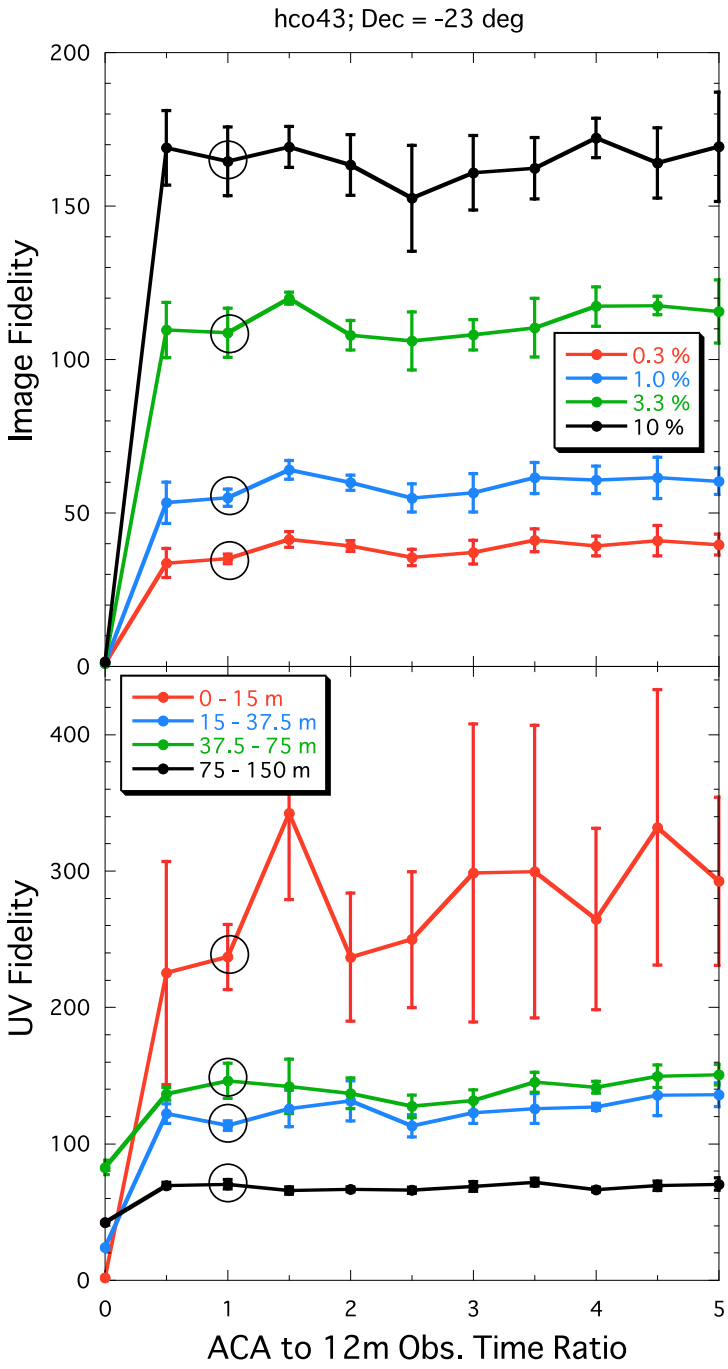

Fig. 9. Dependence of the imaging fidelity (upper panel) and *uv* fidelity (lower) on the ratio between the ACA observing time to the 12-m array observing time. The model image is "hco43" at the declination of -23°. The hour angle coverage of the 12-m array is fixed to -0.5 – 0.5 (hour), and the hour angle coverage of the ACA is $-0.5X$ – $0.5X$ (hour), where X is in the abscissa. Red, blue, green, and black circles in the upper panel show the averaged values of the median imaging fidelity with a lower flux cutoff level of 0.3, 1, 3.3 and 10% of the peak, while those in the lower panel the averaged values of the median *uv* fidelity with a *uv* distance of 0 – 15 m, 15 – 37.5 m, 37.5 – 75 m, and 75 – 150 m, respectively. Error bars show the rms variations for 5 repetitions of the simulations. Open circles indicate the overlapping data point of the subsequent simulations shown in Figure 12, with the same simulation parameters.

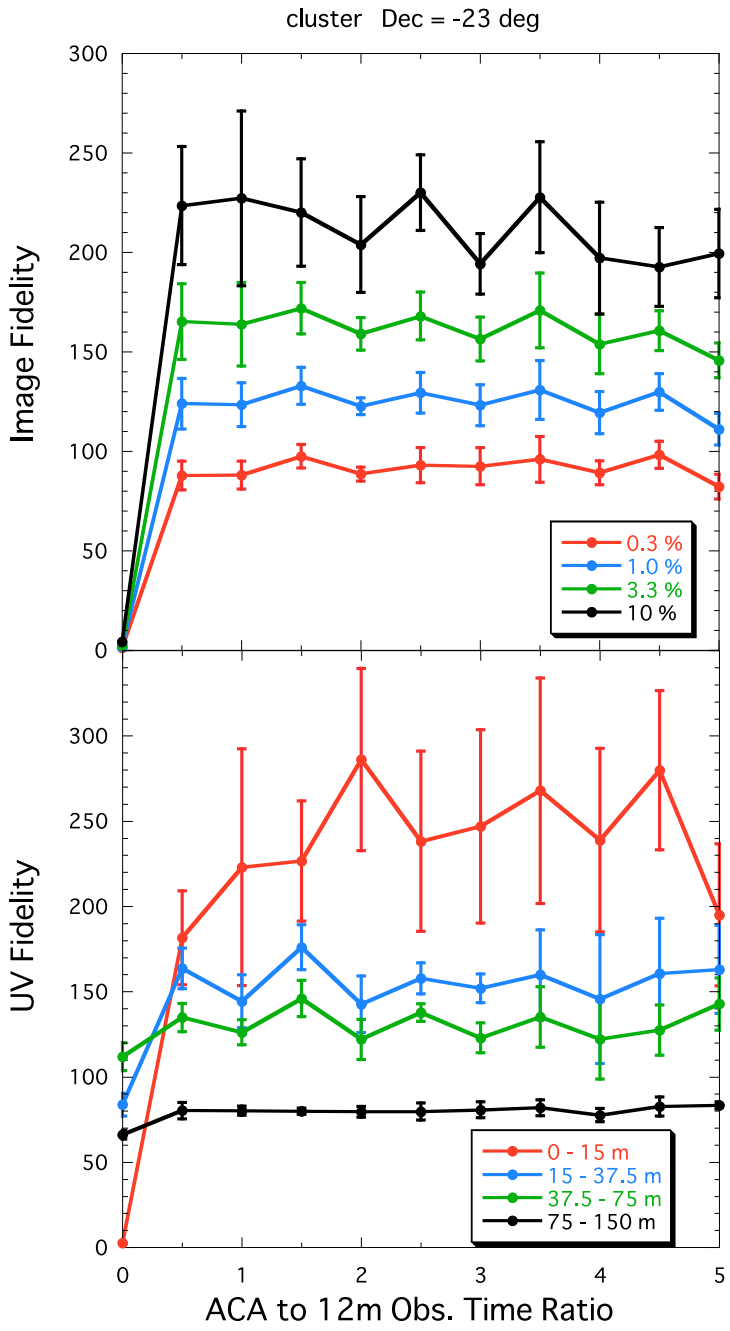

Fig. 10. Same as Figure 9 but for the "cluster" model image.

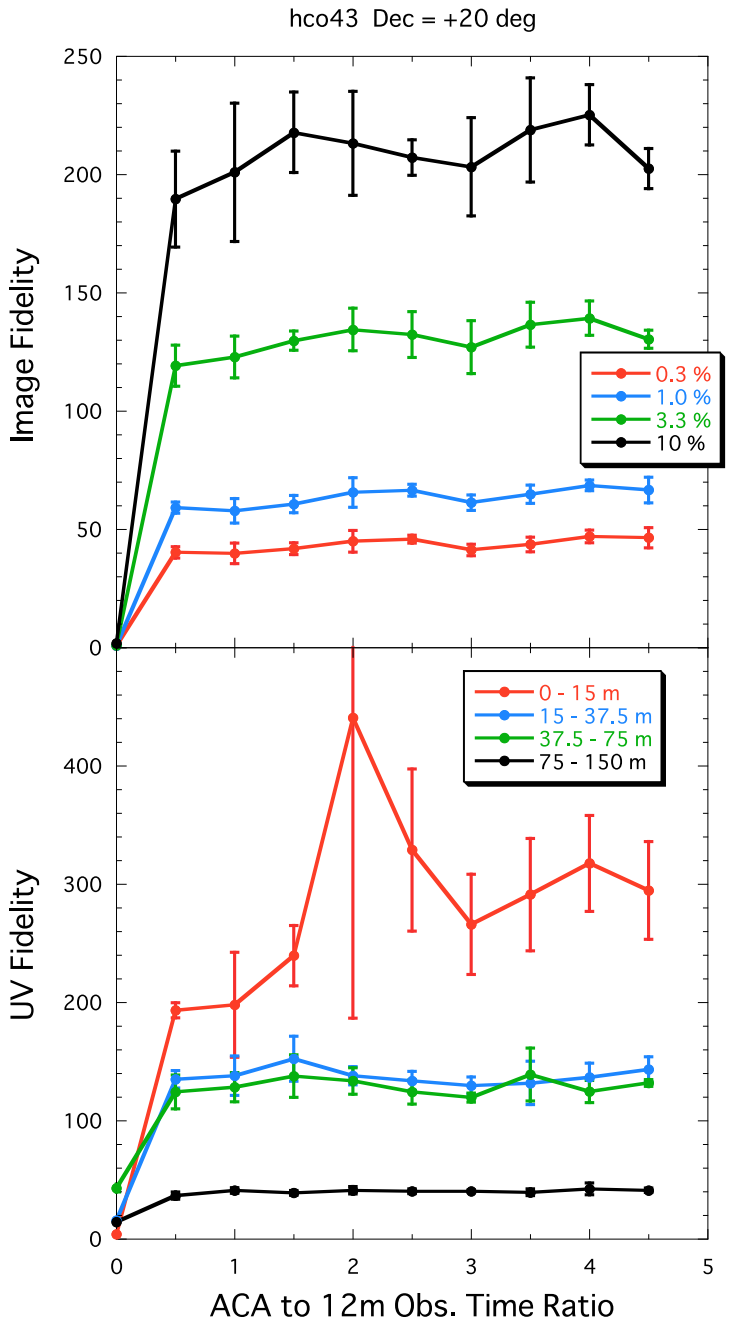

Fig. 11. Same as Figure 9 but at the declination of +20°.

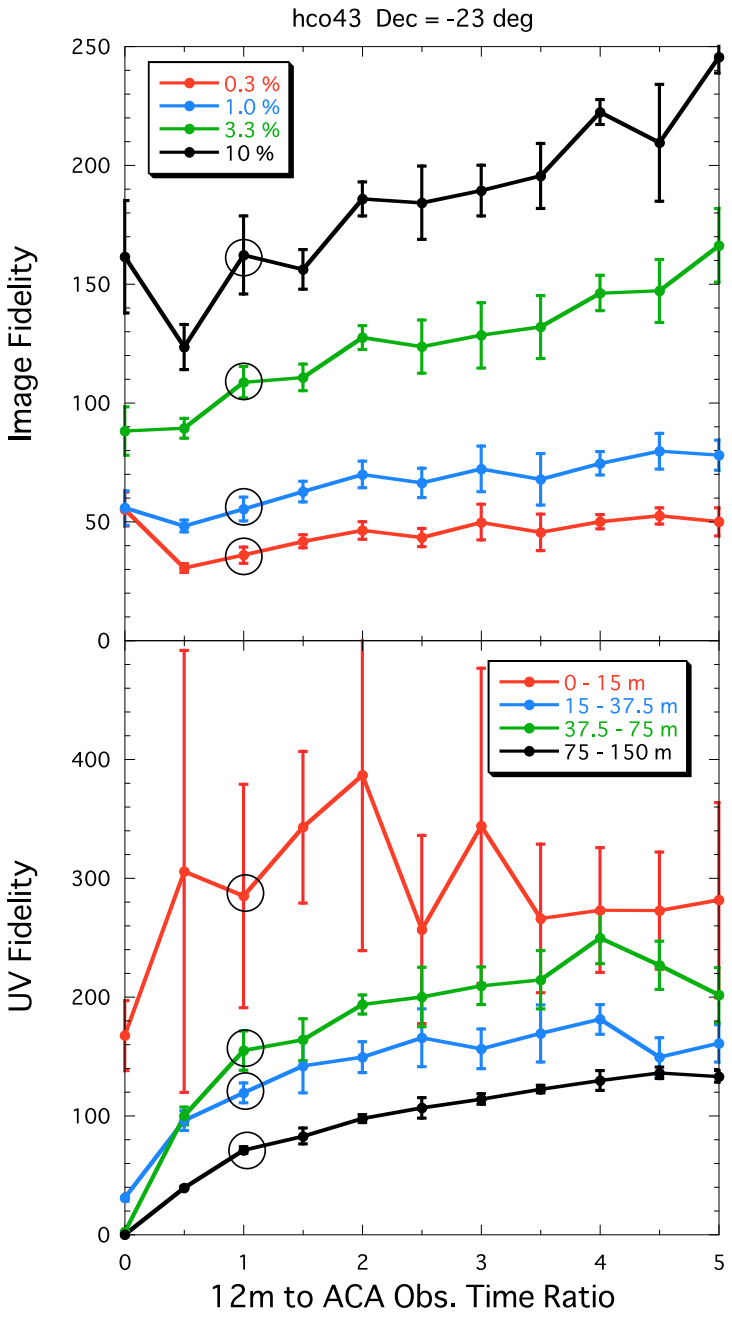

Fig. 12. Dependence of the imaging fidelity (upper panel) and *uv* fidelity (lower) on the ratio between the 12-m array observing time to the ACA observing time. The model image is "hco43" at the declination of -23°. The hour angle coverage of the ACA is fixed to -0.5 – 0.5 (hour), and the hour angle coverage of the 12-m array is -0.5X – 0.5X (hour), where X is in the abscissa. Red, blue, green, and black circles in the upper panel show the averaged values of the median imaging fidelity with a lower flux cutoff level of 0.3, 1, 3.3 and 10% of the peak, while those in the lower panel the averaged values of the median *uv* fidelity with a *uv* distance of 0 – 15 m, 15 – 37.5 m, 37.5 – 75 m, and 75 – 150 m, respectively. Error bars show the rms variations for 5 repetitions of the simulations. Open circles indicate the overlapping data point of the previous simulations shown in Figure 9, with the same simulation parameters.

Table 2. Median Imaging Fidelities at the 1 % Cutoff Level

Model Image	12-m Array only	12-m Array plus TP Array[a]	ACA only	All (ACA × 1)[b]	All (ACA × 4)[c]
hco43 (δ = -23°)	0.93 ± 0.00	9.08 ± 0.29	55.82 ± 7.25	54.96 ± 2.83	60.71 ± 4.48
hco43 / 500 [d] (δ = -23°)	0.97 ± 0.01	6.26 ± 1.41	3.97 ± 0.59	5.25 ± 0.63	8.29 ± 0.81
hco43 (δ = +20°)	0.87 ± 0.00	20.23 ± 2.30	52.91 ± 8.45	57.90 ± 5.23	64.84 ± 3.79
hco43 / 500 [d] (δ = +20°)	0.75 ± 0.01	7.26 ± 1.08	5.20 ± 1.12	6.47 ± 0.96	8.40 ± 0.57
cluster (δ = -23°)	1.74 ± 0.01	102.96 ± 13.30	81.22 ± 7.97	123.47 ± 11.02	119.46 ± 10.66
cluster / 100 [e] (δ = -23°)	1.46 ± 0.04	10.04 ± 1.33	7.17 ± 2.32	11.9 ± 3.43	16.26 ± 1.55

a: Imaging simulations with the 12-m array and the ACA total power array.

b: Imaging simulations with the 12-m array, the ACA 7-m array and the ACA total power array, where the hour angle coverage of the ACA 7-m array is same as that of the 12-m array (from -0.5 hour to +0.5 hour).

c: Imaging simulations with the 12-m array, the ACA 7-m array and the ACA total power array, where the hour angle coverage of the ACA 7-m array (from -2.0 hour to +2.0 hour) is four times more than that of the 12-m array (from -0.5 hour to +0.5 hour).

d: The input model is "hco43", but the flux is reduced by a factor of 500.

e: The input model is "cluster", but the flux is reduced by a factor of 100.

15. Contrary to the high S/N case, the imaging fidelities and *uv* fidelities at short spacings (< 37.5 m) improve as the ACA observing time increases. Although the rms variations from the 5 repetitions are rather large, the improvement of the imaging can be seen clearly in the fidelity images shown in Figure 16 and 17. We note that in Figure 16 and 17 the images of the difference show systematic patterns with the ACA-to-12-m ratio of 1, while the images are random-like noise with increased ACA observing time. This result may imply that the deconvolution algorithm cannot recover the image structures well with less ACA observing time in the low S/N case, and that the solutions depend on the parameters of the deconvolution algorithm or the adopted algorithm itself. Table 2 summarizes median imaging fidelities of these simulations with a cutoff level of 1 % of the peak. Varying the 12-m observing time as compared to the ACA observing time also improves the image at longer spacings (> 15 m) in the low S/N case (Figure 18).

4. Discussion

4.1. Implications of our Simulations

Our simulations suggest that in the high S/N case the imaging fidelity does not improve as the ACA observing time increases, and in the low S/N case the fidelity improves monotonically. Increasing the 12-m array observing time improves the imaging monotonically in the noise-free case, and slightly in the low S/N case. These results can be interpreted as follows:

- Noise-Free Case: For high S/N cases, the deconvolution algorithms are efficient enough to satisfactorily recover most of the flux even for observing time ratios of 1:1 between both arrays. The final achievable fidelity is mainly controlled by the amount of power in the high spatial frequency components of the target, and thus by the observing time of the 12m Array. The addition of the ACA data is, though, essential to improve the fidelities (see Table 2).

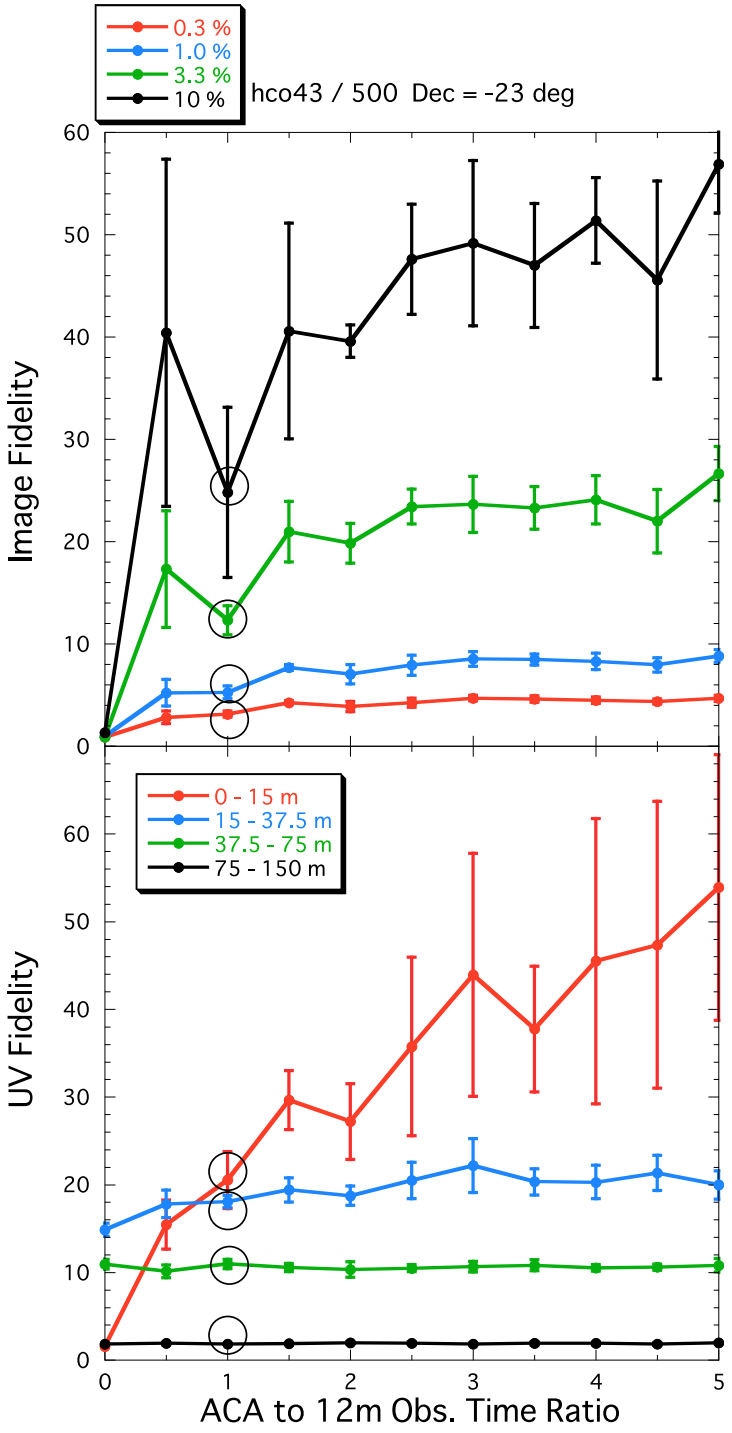

Fig. 13. Same as Figure 9, but the flux of the model image is reduced by a factor of 500.

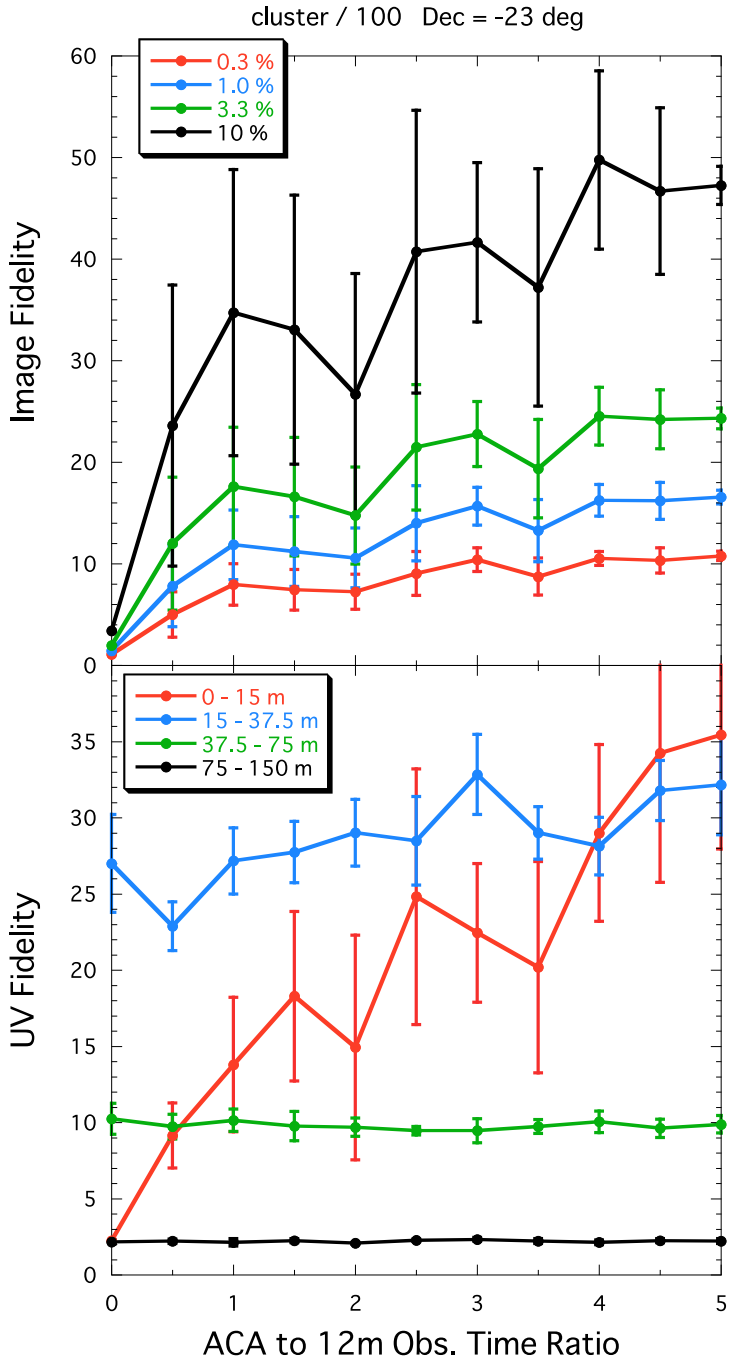

Fig. 14. Same as Figure 10, but the flux of the model image is reduced by a factor of 100.

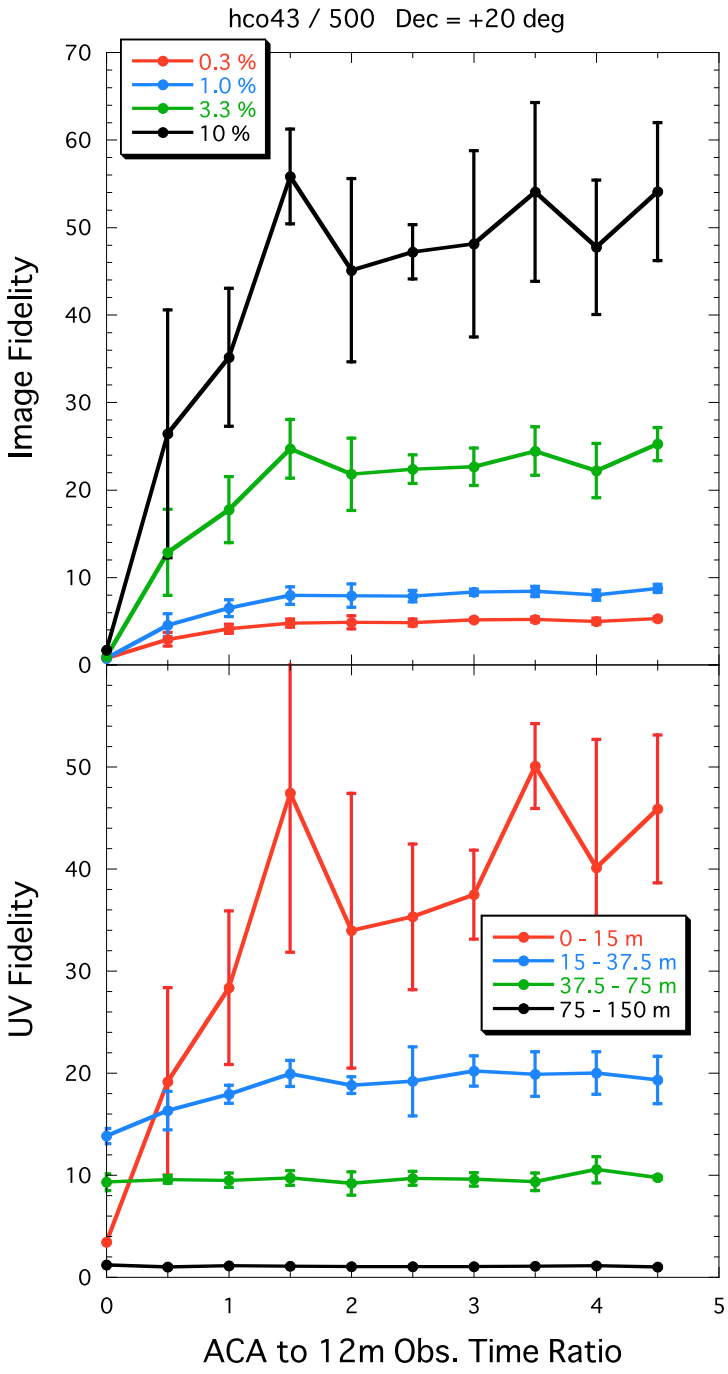

Fig. 15. Same as Figure 13, but for the declination of +20°.

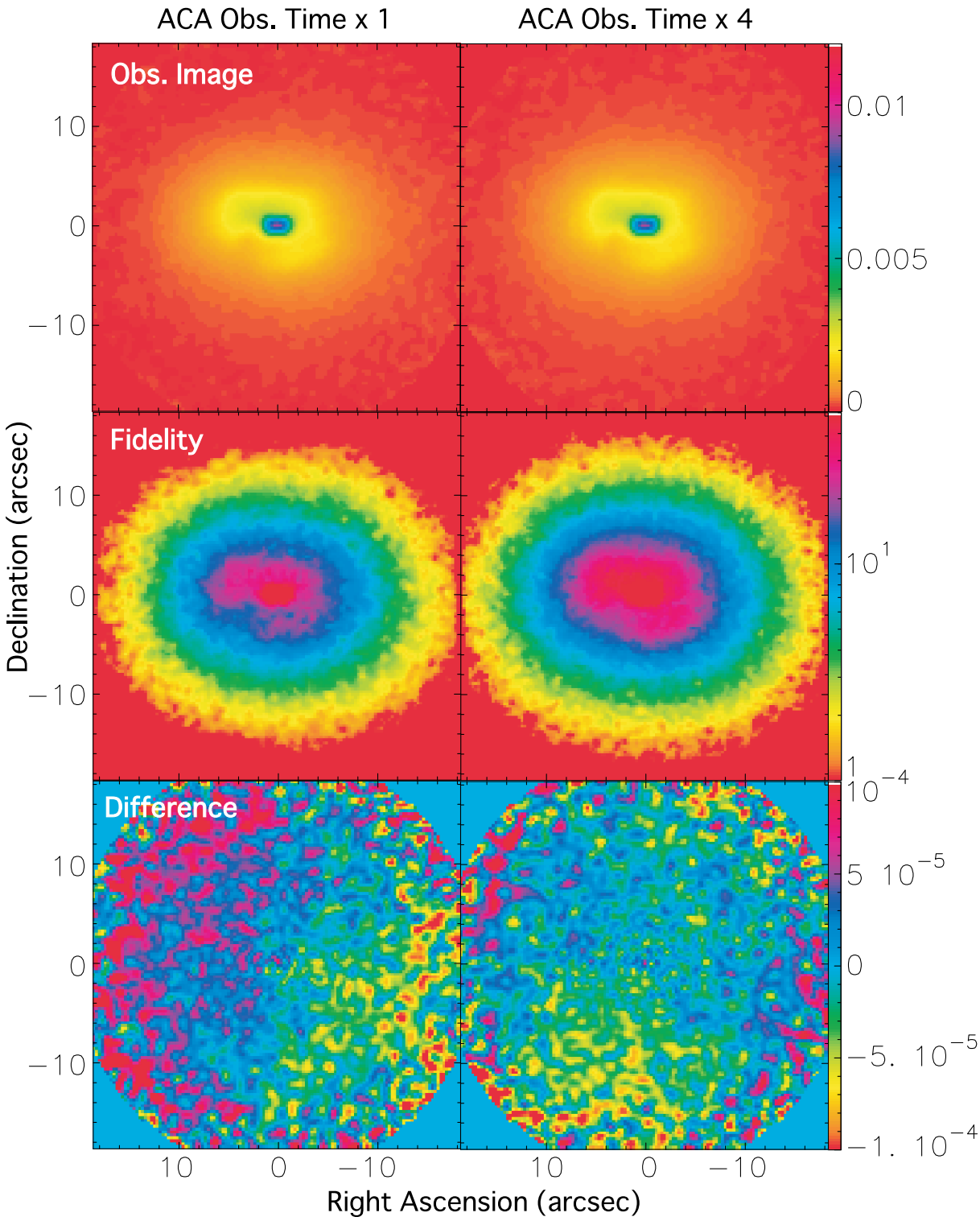

Fig. 16. Averaged images of the simulated observation (top panels), fidelity (middle), and the difference between the simulated image and the model (bottom), from 5 repetitions of the imaging simulations. The model image is "hco43", but the flux is reduced by a factor of 500. The source declination is -23°. In the left panels, the hour angle coverage is -0.5 – 0.5 (hour) for both the 12-m array and the ACA, while in the right panels the hour angle coverage of the ACA is changed to be -2.0 – 2.0 (hours).

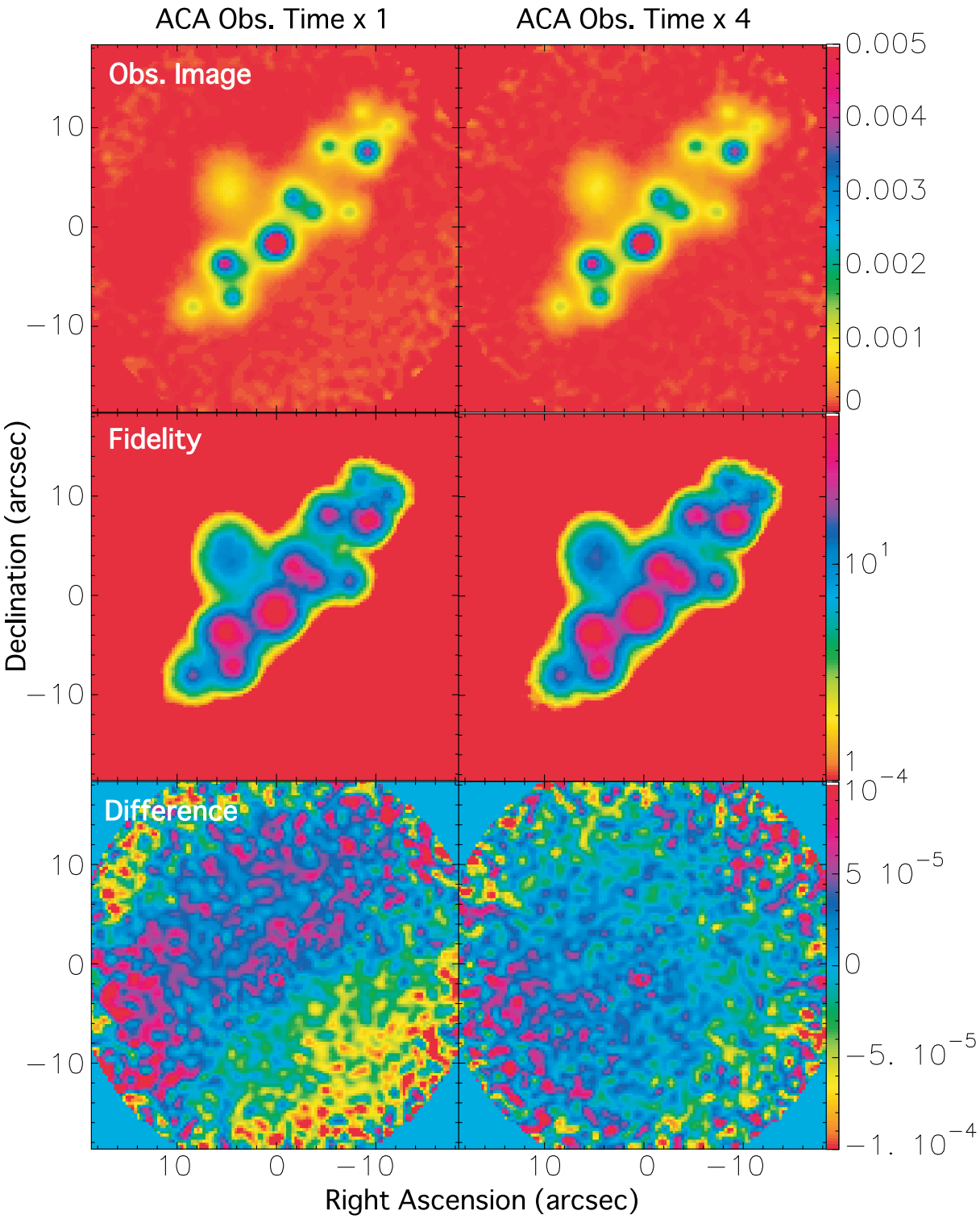

Fig. 17. Same as Figure 16, but for the "cluster" model image with the flux reduced by a factor of 100.

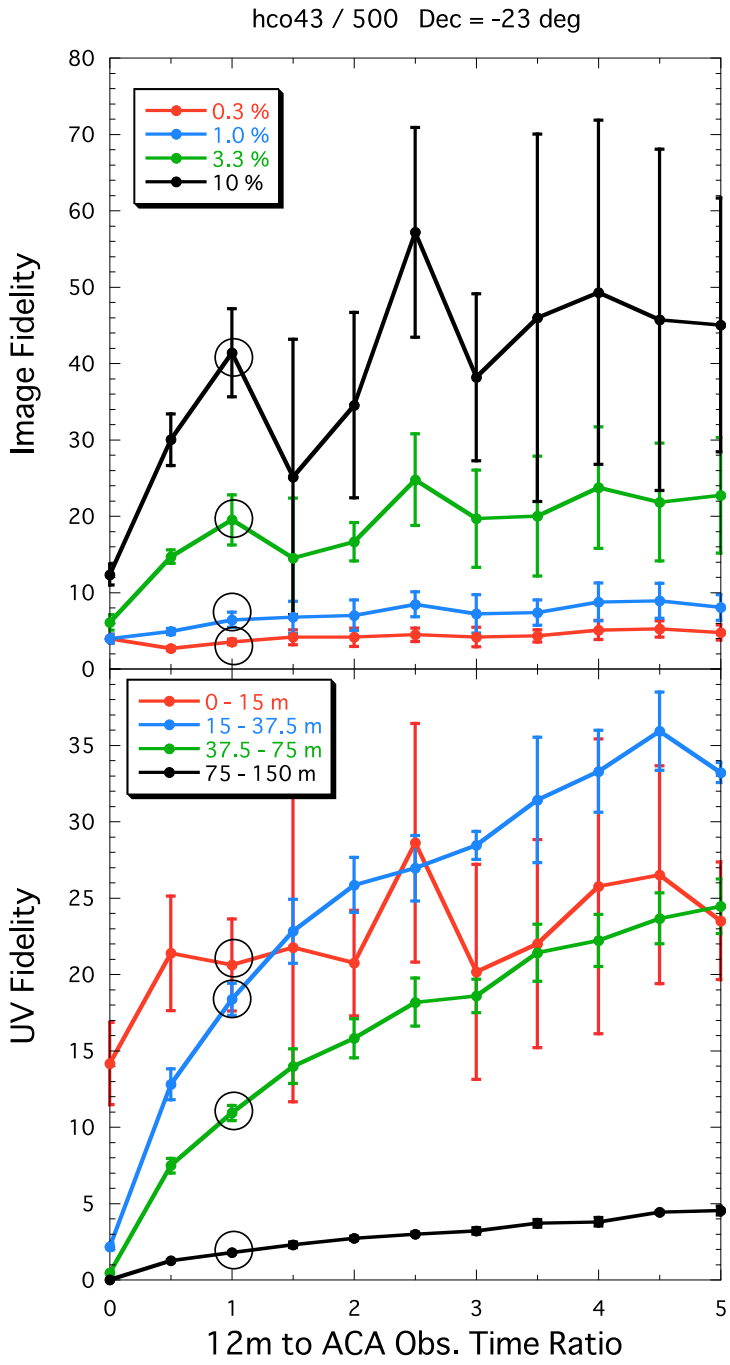

Fig. 18. Same as Figure 12, but for the flux reduced by a factor of 500.

- Low S/N Case: The fidelities follow an increase with observing time ratio. This suggests that, in fact, for the sources used, the ACA data is dominating the fidelities (due to the relatively small amount of power that the model sources have in the high spatial frequency components). For such sources, the use of a subarray of the 12m Array in Total Power mode may improve the fidelities significantly.
- Source Properties: Although the sources selected for the simulations represent some extreme cases (in Pety et al 2001, the "hco43" image usually shows a high fidelity improvement if the ACA is added, while in the case of the "cluster" image the improvement is marginal), there is no difference in overall conclusions between the two models.

The results above suggest that no optimum ratio of observing times between the ACA and the 12m Array was found, and that the analytical estimate of $\times 4$ factor that had been used so far to estimate relative observing times is not necessary to achieve the improvement of image fidelity that the ACA provides. The factor 4 has been derived from matching uv point-source sensitivity in the overlapping baseline regions between the 12-m array and the ACA, including the assumption of mosaicking observations. In the linear analytical regime this value is still valid and we do not argue against it. However, our simulations show that in the non-linear regime including deconvolution the analytical estimate is not sufficient to make a firm conclusion. If this factor 4 were correct, the fidelity should increase and saturate at the ACA-to-12-m observing time ratio of 4, but this is not what our results show.

One probable reason for the noise-free case is that the ACA samples only short-spacing information, where the source flux is stronger and the source structure simpler, and with a limited hour angle coverage we can obtain a denser uv-coverage than that of the 12-m array with longer baselines (See Figure 2 and 3). The stronger flux means that with short integration times with the ACA we can achieve the same signal-to-noise ratio as that of the 12-m array in the uv-domain, and the simplicity of the source structure enables the deconvolution algorithm to recover the structure and the flux correctly. The improvement of the imaging fidelity as a function of the 12-m observing time supports this argument, since the 12-m array covers much wider uv-regions and the increment of the 12-m Hour-Angle coverage improves the uv-coverage significantly. In case there is a requirement for high fidelity of the high spatial-frequency components, the 12m Array time should be increased with respect to that of the ACA.

For weak sources, the ACA dominates the fidelities, and therefore, fidelities will increase as the observing time of the ACA increases. The 12m Array might provide support in terms of improved spatial resolution and additional total power observations. Target sources will usually be somewhere between these two regimes.

Adding these results to the advantages of a "combined" mode of operation one must conclude that a more central role of the combined array mode for ALMA should be seriously considered. For sources that do not require mosaicking, the advantages would be in terms of calibration and increased sensitivity. For extended sources, significant fidelity improvements

can be expected even with a 1:1 observing time ratio. Studies should therefore be started on the impact that a more important role of the combined mode will have to ALMA operations.

4.2. Cautions

Although the current results seem fairly robust, there are several issues that still need to be addressed. First, we have to increase the number of model sources to confirm these results. Using other packages to carry out similar simulations is also important. The GILDAS package treats differently the "homogeneous" mosaicking with Single-Dish data and the ACA+Single-Dish+12m Array case. All deconvolutions have been done with a modified CLEAN algorithm in the hybrid mode (separate deconvolution of ACA+SD and ALMA datasets that are then combined in the uv plane). We should investigate how the deconvolution affects the main results, with other imaging packages such as MIRIAD. In addition, the GILDAS simulator cannot take cross correlation between the 12-m array and the ACA, and hence it is also important to conduct imaging simulations with the cross correlation between the 12-m array and the ACA. We can also tweak the single-dish integration time to find the optimal value. It is also important to include additional errors such as phase screens, and different array configurations of the 12-m array, to make more "realistic" simulations.

5. Conclusions

We have made ALMA imaging simulations using GILDAS to investigate the optimal ACA observing time as compared to the 12-m observing time. For the source structures adopted in our simulations there is no clear optimal ACA observing time with a fixed 12-m array observing time. These simulation results imply that we need to seriously consider the use of the combined array as well in the ALMA operation.

References

Conway, J. 2005, ALMA-90.02.00.00-006-A-SPE

Holdaway, M. A., & Morita, K. 2006, to be appeared in the ALMA memo

Morita, K., & Holdaway, M. A. 2005, ALMA Memo 538

Pety, J., Gueth, F., & Guilloteau, S. 2001a, ALMA Memo 386

Pety, J., Gueth, F., & Guilloteau, S. 2001b, ALMA Memo 387

Pety, J., Gueth, F., & Guilloteau, S. 2001c, ALMA Memo 398

Sault, R. J., Teuben, P. J., & Wright, M. C. H. 1995, Astronomical Data Analysis Software and Systems IV, ASP Conference Series, Vol. 77, R. A. Shaw, H. E. Payne, & J. J. E. Hayes, eds., p.433

Tsutsumi, T., Morita, K., Hasegawa, T., & Pety, J. 2004, ALMA Memo 488